these features would enable true single-molecule measurements over arbitrarily long times.

In this work, we have estimated the temperature rise of metal particles 5 nm in diameter at about 15 K. The temperature rise declines as the reciprocal distance from the particle's center, decreasing to 3 K at a distance of 13 nm from the center. Although small, this temperature increase might still be too high for some proteins or biomolecules. We believe, however, that the S/N can be substantially improved in a transmission geometry and by reaching the photon noise limit in detecting the probe beams. The label heating could then be reduced by a factor of 10 and would become negligible for most biomolecules at ambient conditions.

References and Notes

1. W. E. Moerner, M. Orrit, *Science* **283**, 1670 (1999).
2. M. Bruchez Jr., M. Moronne, P. Gin, S. Weiss, A. P. Alivisatos, *Science* **281**, 2013 (1998).
3. W. C. Chan, S. Nie, *Science* **281**, 2016 (1998).
4. M. Nirmal *et al*., *Nature* **383**, 802 (1996).
5. M. P. Sheetz, S. Turney, H. Qian, E. L. Elson, *Nature* **340**, 284 (1989).
6. W. Baschong, J. M. Lucocq, J. Roth, *Histochemistry* **83**, 409 (1985).
7. J. W. Slot, H. J. Geuze, *Eur. J. Cell Biol.* **38**, 87 (1985).
8. P. A. Frey, T. G. Frey, *J. Struct. Biol.* **127**, 94 (1999).
9. J. F. Hainfeld, R. D. Powell, *J. Histochem. Cytochem.* **48**, 471 (2000).
10. S. Schultz, D. R. Smith, J. J. Mock, D. A. Schultz, *Proc. Natl. Acad. Sci. U.S.A.* **97**, 996 (2000).
11. J. Gelles, B. J. Schnapp, M. P. Sheetz, *Nature* **331**, 450 (1988).
12. C. Sönnichsen *et al*., *Appl. Phys. Lett.* **77**, 2949 (2000).
13. J. M. Robinson, T. Takizawa, D. D. Vandre, *J. Microsc.* **199**, 163 (2000).
14. C. F. Bohren, D. R. Huffman, *Absorption and Scattering of Light by Small Particles* (Wiley, New York, 1983).
15. M. Tokeshi, M. Uchida, A. Hibara, T. Sawada, T. Kitamori, *Anal. Chem.* **73**, 2112 (2001).
16. P. Cleyzes, A. C. Boccara, H. Saint-Jalmes, *Opt. Lett.* **22**, 1529 (1997).
17. If cells or other bulk samples were studied, the two transmitted red beams would have to recombine in a second Wollaston prism. Here, to demonstrate photothermal detection of metal particles on surfaces, we used the weaker beams reflected by the glass substrate at the expense of the final signal and S/N ratio.
18. H. S. Carslaw, J. C. Jaeger, *Conduction of Heat in Solids* (Oxford Univ. Press, Oxford, ed. 2, 1986).
19. T. Klar *et al*., *Phys. Rev. Lett.* **80**, 4249 (1998).
20. We thank D. Choquet for helpful discussions, L. Cognet for valuable help with the DIC setup, and J.-M. Turlet for various equipment. Funding of this work by CNRS (Individual Nano-Object program), Région Aquitaine, and the French Ministry for Education and Research (MENRT) is gratefully acknowledged.

9 May 2002; accepted 8 July 2002

Electron Solvation in Two Dimensions

A. D. Miller,[1] I. Bezel,[2] K. J. Gaffney,[1]* S. Garrett-Roe,[1] S. H. Liu,[1] P. Szymanski,[1] C. B. Harris[1]†

Ultrafast two-photon photoemission has been used to study electron solvation at two-dimensional metal/polar-adsorbate interfaces. The molecular motion that causes the excess electron solvation is manifested as a dynamic shift in the electronic energy. Although the initially excited electron is delocalized in the plane of the interface, interactions with the adsorbate can lead to its localization. A method for determining the spatial extent of the localized electron in the plane of the interface has been developed. This spatial extent was measured to be on the order of a single adsorbate molecule.

The interaction of excess electrons at interfaces is not only of fundamental interest, but affects processes such as charge injection and transport in molecular electronics and electrochemistry (*1, 2*). Electron solvation represents a general interaction of an electron with its surroundings. In the broadest sense, electron solvation occurs when the molecules surrounding an electron reorganize to accommodate the electron's charge density. Although extensive investigations of solvation in isotropic media have been conducted (*3–7*), comparatively little is known about the dynamics of electron solvation at metal/molecular interfaces. Both the reduced dimensionality and hindered solvent motion could lead to dynamics distinct from those of isotropic materials (*8–11*).

We present the results of an ultrafast two-photon photoemission (TPPE) investigation of electron solvation dynamics at an interface consisting of a two-dimensional (2D) layer of polar molecules on a single-crystal metal surface. Ultrafast TPPE is a pump-probe technique used to observe the electronic structure and dynamics of electrons at metal surfaces and interfaces (*12–16*). The pump pulse promotes electrons from below the Fermi level to initially unoccupied interfacial states. The probe pulse photoemits the electrons, the kinetic energy of which is measured (Fig. 1A). A time delay between the arrival of the pump and the probe pulse is used to determine the dynamic properties of the system. Two experimental signatures associated with the electron solvation dynamics at polar-adsorbate/metal interfaces were identified. The first is the time-dependent shift in electronic energy due to molecular reorientation at the interface in the presence of the electron. The second is the dynamic localization of interfacial electrons by the dipole layer. The first effect resembles the time-dependent Stokes shift seen in numerous studies of solvation dynamics in the liquid phase. The second effect is associated with the ability of electrons photoexcited to states delocalized in the plane of the interface to localize if the solvent dipole-layer distortion leads to the formation of an energetically favorable site.

We used TPPE to investigate electron solvation and the resulting localization dynamics on acetonitrile/Ag(111) and butyronitrile/Ag(111) interfaces. The instrument function of the laser at the 1.7 to 1.9 eV probe and the 3.4 to 3.8 eV second-harmonic pump photon energies used was ~100 fs. The two nitriles have molecular dipole moments of 3.9 and 3.7 Debye, respectively (*17, 18*). The layer-by-layer growth of the nitriles on the Ag(111) surface has been confirmed with TPPE, which produced distinctly different spectra for monolayer and bilayer coverages. The layers were adsorbed at temperatures between 100 and 140 K, and the data was collected at a temperature of 80 to 90 K. Electrons in polar molecular glasses still solvate at these temperatures, though on a longer time scale (*19*). Low-energy electron diffraction (LEED) studies of these interfaces lack LEED spots, demonstrating the absence of long-range translational order. Similar conclusions have been drawn from near edge x-ray absorption fine structure experiments for acetonitrile adsorbed on Ag(110) (*20*) and Au(100) (*21*) and LEED experiments on acetonitrile/Au(100) (*22*). Acetonitrile has a negative electron affinity of –2.8 eV (*23*), indicating that the image potential state electrons should be pushed out to the layer/vacuum interface and not interact with the electronic structure of the layer.

TPPE was used to populate the electron's image potential states and observe their subsequent dynamics. Image potential states result from the attractive interaction between an electron outside of a surface and the surface polarization that it induces. The resultant Coulomb potential supports an infinite series of hydrogenic states confined normal to the surface (*13, 24, 25*). Parallel to the surface,

[1]Department of Chemistry, University of California, Berkeley, and Chemical Sciences Division, E. O. Lawrence Berkeley National Laboratory, Berkeley, CA 94720, USA. [2]Miller Institute for Basic Research in Science, 2536 Channing Way #5190, Berkeley, CA 94720, USA.

*Present address: Department of Chemistry, Stanford University, Stanford, CA 94305, USA.

†To whom correspondence should be addressed. E-mail: harris@socrates.berkeley.edu

the electron is free to move and thus delocalize over a substantial area. For metal surfaces, the energies of image potential states in electron volts are given by

$$E_n = V_0 - \frac{0.85}{(n + a)^2} \quad (1)$$

where n is the principle quantum number and a is the quantum defect parameter. The series converges to V_0, the vacuum energy for a uniform surface. Electrons in image potential states reside only a few angstroms outside the interface, making them particularly sensitive to changes in the interfacial electrostatic potential, V_0. This is illustrated schematically in Fig. 1B.

The kinetic energy of both the $n = 1$ and the $n = 2$ image potential states for a monolayer of acetonitrile decrease as a function of time (Fig. 2). Similar dynamics have also been observed for butyronitrile and primary alcohols, ranging from methanol to 1-pentanol. While the absolute photoelectron kinetic energy, E_{kin}, changes on the time scale of hundreds of femtoseconds, the energy spacing between the $n = 1$ and $n = 2$ image potential states remains nearly constant. A constant energy spacing indicates that the binding energies of the image potential states, as defined by the second term in Eq. 1, do not change with time. Instead, the time-dependent kinetic energies result from a time-dependent variation of the potential V_0. This time dependence is attributed to a change in the electrostatic field produced by the rearrangement of the molecular dipoles in the vicinity of the delocalized electron. This rearrangement lowers the electron energy and reduces the local workfunction (*26*).

The presence of an electron in a low-lying image state greatly perturbs the electrostatic potential experienced by the dipolar layer, and vice versa. The adsorbates respond to the perturbation by rotating the positive end of their molecular dipoles toward the electron. This reorientation results in an increased projection of the molecular dipole along the surface normal and causes a reduction in the local workfunction. Stabilization of the electron at the interface may therefore be viewed as a dynamically decreasing local workfunction induced by the electron's interaction with the reorienting molecular dipoles in the adsorbate layer (Fig. 1C). The local workfunction change from a reorientation of a patch of the acetonitrile layer can be modeled by representing the collection of dipoles by a pair of charged disks. This model results in a local workfunction shift as large as 1.5 eV. The molecular reorientation of the monolayer is not complete before the electrons have decayed into the metal. The observed 0.27 eV dynamic shift, although not complete, falls within the range of the model. In liquids, acetonitrile has been observed to reorient on an electrode surface when subject to strong electric fields (*27*). Here, the electron in the image potential state produces such a field initiating the reorientation.

The ultrafast reorientation of the molecular dipoles can also cause an initially delocalized electron to dynamically localize. The spatial extent of excited electronic states parallel to the surface can be determined by measuring E_{kin} as a function of the angle, θ, between the sample surface normal and the direction toward the detector. The projection of the electron momentum on the surface, $p_{||}$, is conserved during photoemission and is given by

$$p_{||} = \sqrt{2E_{kin}m_e}\, sin\theta \quad (2)$$

where m_e is the free electron mass. E_{kin} is given by

$$E_{kin} = E_{||} + \hbar\omega - E_n = \frac{p_{||}^2}{2m^*} + \hbar\omega - E_n \quad (3)$$

where $E_{||}$ is the kinetic energy of electron motion parallel to the surface while in the interfacial state, m^* is the electron's effective mass and $\hbar\omega$ is the photon energy. Nearly free electron states have m^* approximately equal to m_e, whereas localized electronic states have $m^* \gg m_e$ and hence E_{kin} is independent of $p_{||}$ and θ. The energy of a delocalized electron increases parabolically with increasing $p_{||}$ whereas the energy of a localized electron does not change markedly with $p_{||}$ (Eq. 3).

Figure 3 shows TPPE spectra of a bilayer of butyronitrile/Ag(111) as a function of time. At $t = 0$ fs, the $n = 1$ image potential state is delocalized, while at $t \sim 300$ fs the delocalized state is apparent as well as a new state. The latter has a $p_{||}$-independent energy, indicative of an image potential state localized parallel to the surface. At $t > 1$ ps, only the localized state remains. Figure 4 plots the intensity of the delocalized and the localized $n = 1$ states of the bilayer of butyronitrile as a function of time at $\theta = 16.4°$. The population evolution can be followed by using TPPE, which shows how the localized state is populated by the delocalized state. The energy of both the delocalized and localized electron decreases because of the molecular reorientation. For the localized electron, this is 2D solvation. For the delocalized electron, the stabilizing molecular reorganization is analogous to solvation, but without the accompanying localization. The time scales for the energy shifts of both the localized and the delocalized states are almost the same. This result suggests that the same type of molecular motion, molecular dipole rotation, is responsible for the solvation of both states.

An important feature of the nitrile systems

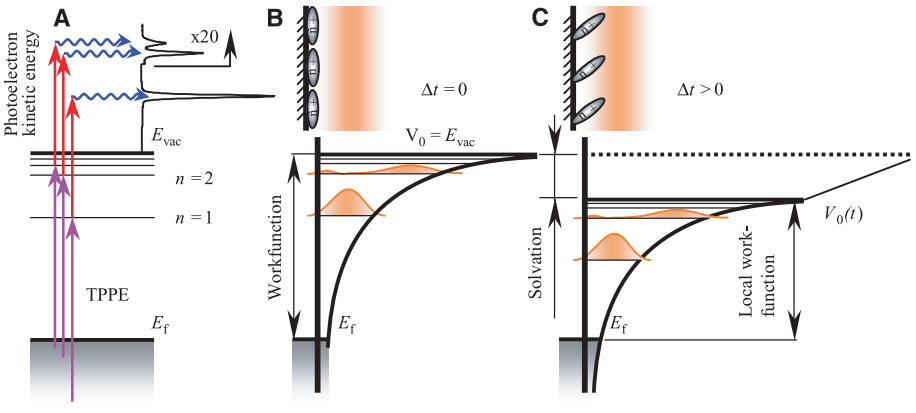

Fig. 1. (**A**) Schematic of the TPPE experiment. Vertical arrows show photoinitiated transitions from below the Fermi level (E_f) to the interfacial image potential states and to the free electron states above the vacuum energy (E_{vac}). The kinetic energy spectrum reflects the interfacial electronic structure. (**B**) Shown are the image potential (thick black solid curve) and the first few image potential states at the first moment after excitation, when the solvent did not have time to reorient. The image state progression converges to E_{vac}. (**C**) Same as (B), but after the solvation took place. The local surface potential V_0 and the local workfunction are lowered by solvation effects.

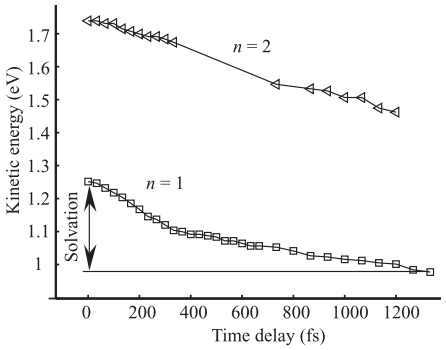

Fig. 2. The $n = 1$ and $n = 2$ image potential state energies as a function of delay time for a monolayer of acetonitrile on Ag(111). The energy difference between the two states is nearly constant as a function of time, indicating that the shift is a result of a change in the local workfunction and not a change in the binding energy.

is that localization phenomena only occur at coverages in excess of a monolayer. For the coverage of one monolayer, no localized state was observed. Localization in two dimensions results from a subtle balance between the propensity for electrons to localize or remain delocalized (*28, 29*). This is reflected in the small self-trapping energy (the energy difference between the delocalized and localized states), as can be seen in the 0° spectra from Fig. 3B. Small differences in the layer's reorganization energy, due to structural differences between the monolayer and bilayer, can tip this balance one way or the other.

Theoretical considerations have predicted that the balance of forces that drive localization will change dramatically as a function of a system's dimensionality. Theory suggests that in 2D crystals, if a charge localizes, it localizes to a single lattice site (*30–32*). Angle-resolved TPPE measurements can directly probe the wave function of the 2D localized state (see supporting online text). When spatially localized in the plane of the surface, electrons acquire a spread in momentum space, according to the uncertainty principle, and the signal intensity as a function of $p_{\|}$ is a reflection of the probability amplitude for the electron to have this $p_{\|}$ in the localized state. The spread of the electron wave function can be estimated from the $p_{\|}$-dependent amplitude of the localized state. In the approximation that the photoemission final states are plane waves, the photoemission probability is directly proportional to the spatial Fourier transform of the electron density, $|\psi(p_{\|})|^2$. The shape of the electron wave function in the momentum space is unchanged after about 100 fs and has a Gaussian profile (Fig. 5). It corresponds to an electron localization size of ~12 Å full width at half maximum (FWHM), approximately the size of a single butyronitrile molecule. This measurement thus represents a direct experimental determination of the spatial extent of electron localization in two dimensions.

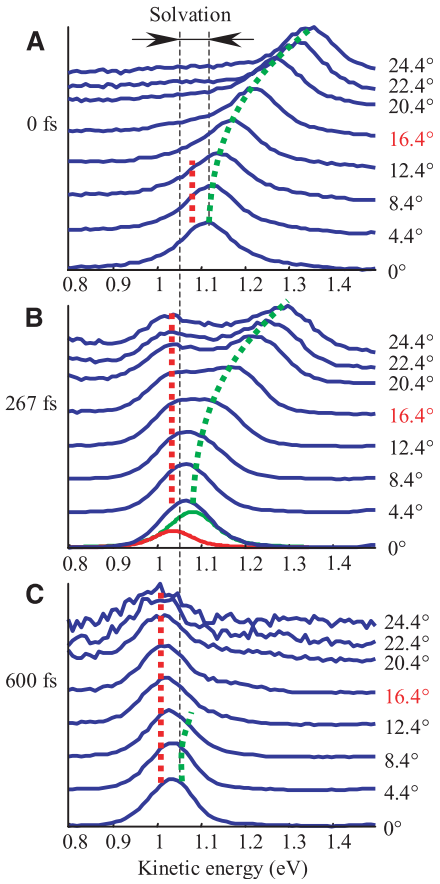

Fig. 3. Photoelectron kinetic energy spectra taken at different observation angles at the delay times between the pump and probe pulses of (**A**) 0, (**B**) 267, and (**C**) 600 fs. The spectra are normalized to unit maximum amplitude and offset vertically by the value of $p_{\|}$. Only the delocalized state is visible at 0 fs delay; both the delocalized and the localized states are equally intense at 267 fs; only the localized state survives past 600 fs. The position of the peaks shifts with time because of solvation. The red and green bell curves in (B) show the contributions of the localized and the delocalized states to the 0° spectrum, respectively. (The positions and widths of the peaks are defined by the fit to the entire dispersion.) The red and green dashed curves in (A) through (C) show their positions at higher angles. The complete dynamics taken at 16.4° is presented in Fig. 4.

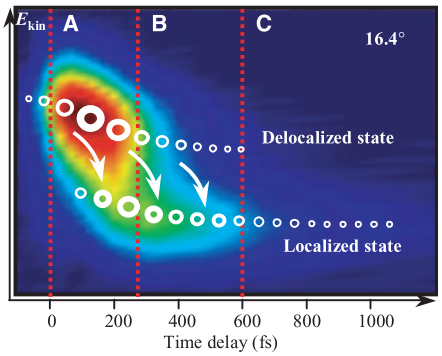

Fig. 4. Dynamics of the localized and the delocalized states. Colors (black through dark red, chosen to better reveal the localized state) represent the amplitude of the signal taken at 16.4° as a function of time and energy. This angle was chosen because the localized and delocalized peaks are sufficiently separated here. Circles show the positions of the localized and delocalized states. The localized state is populated from the delocalized state as indicated by arrows. The three red lines labeled (**A**) to (**C**) show the delay times, at which all angles are presented in Fig. 3, A through C, respectively.

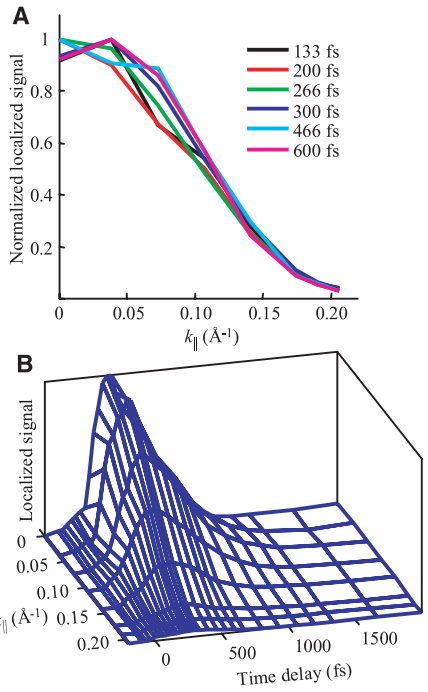

Fig. 5. Localized signal amplitude as a function of $p_{\|}$ and delay time. (**A**) The shape of the localized signal stays constant throughout the dynamics, whereas (**B**) the amplitude grows in the first ~200 fs as the state is populated from the delocalized band and then decays into the substrate. The shape in (A) corresponds to a localized electronic state that is Gaussian with a ~12 Å FWHM in the plane of the surface.

References and Notes

1. D. G. Busch, S. Gao, R. A. Pelak, M. F. Booth, W. Ho, *Phys. Rev. Lett.* **75**, 673 (1995).
2. T. Kugler, M. Logdlund, W. R. Salaneck, *Acc. Chem. Res.* **32**, 225 (1999).
3. R. M. Stratt, M. Maroncelli, *J. Phys. Chem.* **100**, 12981 (1996).
4. G. R. Fleming, M. H. Cho, *Annu. Rev. Phys. Chem.* **47**, 109 (1996).
5. P. J. Rossky, J. D. Simon, *Nature* **370**, 263 (1994).
6. P. K. Walhout *et al.*, *Chem. Phys. Lett.* **232**, 135 (1995).
7. J. A. Kloepfer, V. H. Vilchiz, V. A. Lenchenkov, S. E. Bradforth, *Chem. Phys. Lett.* **298**, 120 (1998).
8. B. J. Loughnane, R. A. Farrer, A. Scodinu, T. Reilly, J. T. Fourkas, *J. Phys. Chem. B* **104**, 5421 (2000).
9. D. M. Willard, R. E. Riter, N. E. Levinger, *J. Am. Chem. Soc.* **120**, 4151 (1998).
10. D. Zimdars, K. B. Eisenthal, *J. Phys. Chem. A* **103**, 10567 (1999).
11. I. Benjamin, *Chem. Rev.* **96**, 1449 (1996).
12. C. B. Harris, N.-H. Ge, R. L. Lingle, J. D. McNeill, C. M. Wong, *Annu. Rev. Phys. Chem.* **48**, 711 (1997).
13. T. Fauster, W. Steinmann, in *Photonic Probes of Surfaces*, P. Halevi, Ed. (Elsevier, Amsterdam, 1995), pp. 347–411.
14. U. Höfer *et al.*, *Science* **277**, 1480 (1997).
15. H. Petek, M. J. Weida, H. Nagano, S. Ogawa, *Science* **288**, 1402 (2000).
16. Q. Zhong, C. Gahl, M. Wolf, *Surf. Sci.* **496**, 21 (2002).
17. D. R. Lide, Ed., *CRC Handbook of Chemistry and Physics* (CRC Press, Boca Raton, FL, ed. 81, 2000).
18. Value is for the *anti* conformer; the *gauche* conformer has a dipole moment of 3.9 debyes.
19. M. Ogasawara, in *Excess Electrons in Dielectric Media*, C. Ferradini, J.-P. Jay-Gerin, Eds. (CRC Press, Boca Raton, FL, 1991), pp. 287–314.
20. P. A. Stevens, R. J. Madix, J. Stohr, *J. Chem. Phys.* **91**, 4338 (1989).
21. T. Soloman, H. Christmann, A. Neumann, J. Baumgärtel, *J. Electroanal. Chem.* **309**, 355 (1991).
22. T. Soloman, H. Christmann, J. Baumgärtel, *J. Phys. Chem.* **93**, 7199 (1989).
23. R. Hashemi, E. Illenberger, *J. Phys. Chem.* **95**, 6402 (1991).
24. P. M. Echenique, J. B. Pendry, *J. Phys. C* **11**, 2065 (1978).
25. N. Memmel, *Surf. Sci. Rep.* **32**, 91 (1998).
26. K. Wandelt, in *Thin Metal Films and Gas Chemisorption*, P. Wissman, Ed. (Elsevier, Amsterdam, 1987), pp. 280–368.
27. S. Baldelli, G. Mailhot, P. Ross, Y. R. Shen, G. A. Somarjai, *J. Phys. Chem. B* **105**, 654 (2001).

28. T. Holstein, *Ann. Phys.* **8**, 343 (1959).
29. D. Emin, T. Holstein, *Phys. Rev. Lett.* **36**, 323 (1976).
30. V. V. Kabanov, O. Y. Mashtakov, *Phys. Rev. B* **47**, 6060 (1993).
31. H. Sumi, A. Sumi, *J. Phys. Soc. Jpn.* **63**, 637 (1994).
32. G. Kalosakas, S. Aubry, G. P. Tsironis, *Phys. Rev. B* **58**, 3094 (1998).

33. We thank C. Wittig for valuable discussions. Supported by the director, Office of Energy Research, Office of Basic Energy Sciences, Chemical Sciences Division of the U.S. Department of Energy, under contract DE-AC03-76SF00098. We acknowledge NSF support for specialized equipment used in these experiments.

Supporting Online Material
www.sciencemag.org/cgi/content/full/297/5584/1163/DC1
SOM Text
References and Notes

3 May 2002; accepted 10 July 2002

Rotationally Resolved Infrared Spectrum of the Charge Transfer Complex $[Ar–N_2]^+$

H. Linnartz,* D. Verdes, J. P. Maier

Difficulties in preparing cluster ions for spectroscopic studies have limited our understanding of intermolecular forces in charged complexes that are typical of many reactive intermediates. Here, the infrared spectrum of the charge transfer complex $[Ar–N_2]^+$, recorded in a supersonic planar plasma with a tunable diode laser spectrometer, is presented. More than 70 adjacent rovibrational transitions were measured near 2272 wave numbers and assigned to the molecular nitrogen stretching fundamental in the $^2\Sigma^+$ ground state of $[Ar–N_2]^+$. The accurate structural parameters that were determined confirm a linear structure and show that the major part of the charge is located at the argon atom. The latter result is surprising and implies a charge switch of the cationic center upon complexation.

A good understanding of intermolecular forces, such as van der Waals interactions or hydrogen bonds, is essential for the description of the chemical and physical properties of matter (*1*). However, although weakly bound neutral complexes have been studied extensively in the past, high-resolution information about polyatomic ionic complexes is limited (*2*). These complexes have binding energies that are typically between those of pure van der Waals and covalent bonds and play a key role as reactive intermediates in many processes. An accurate spectroscopic characterization, therefore, is necessary to understand the structural and dynamical characteristics of cluster ions at the fundamental level of molecular motion.

This is particularly true for the charge transfer complex $[Ar–N_2]^+$, which has been puzzling researchers for two decades. Upon photodissociation, the complex fragments mainly via the decay channel $Ar^+ (^2P_{3/2}) + N_2(X^1\Sigma)$, but the $N_2^+ (X^2\Sigma) + Ar (^1S)$ channel should be energetically preferred (*3*). A similar anomaly is observed in experiments studying the charge transfer process $Ar^+(^2P_{3/2}) + N_2(X^1\Sigma_{v=0}) \rightarrow Ar + N_2^+(X^2\Sigma_{v=v'})$ (*4*). Although the reaction is exothermic by nearly 0.18 eV, its reactivity is typical of that for an endothermic process. These findings indicate that $[Ar–N_2]^+$ is formed in the recombination of Ar with N_2^+ rather than Ar^+ with N_2, but upon photodissociation, the complex fragments into $Ar^+ + N_2$ rather than $Ar + N_2^+$. This special dynamical behavior has been explained in terms of a curve crossing between the states correlating to $N_2^+(X^2\Sigma)/Ar(^1S)$ and $Ar^+(^2P_{3/2})/N_2(X^1\Sigma)$ (*3*). The potential energy surface (PES) of the latter (higher lying) state diabatically correlates to the strongly bound ground state of $[Ar–N_2]^+$, whereas the other (lower lying) state correlates to a repulsive state that is accessed from the ground state by the photon that induces the dissociation [see figure 10 of (*3*)]. Detailed information is now available for the photodissociation and charge transfer dynamics of the $[Ar–N_2]^+$ species, providing state-to-state cross sections, reaction rates, rotational and vibrational energy distributions of the products, and details of the low-lying PES (*3–9*). However, a high-resolution study of the ground state of the reactive intermediate $[Ar–N_2]^+$ has been lacking up to now.

This lack of information is mainly due to the difficulties involved in producing a large abundance of cluster ions under laboratory conditions. Recent progress in the generation of dense supersonic planar plasma expansions has made a more general detection scheme of ionic complexes with direct absorption spectroscopy possible (*10*, *11*). Such a plasma offers a nearly Doppler-free environment and combines high molecular densities and a low final temperature (<20 K) with a relatively long absorption path length. The experimental method applied here is based on the absorption of tunable infrared radiation in a planar plasma that is generated by electron impact ionization with the use of a supersonic ion jet diode laser spectrometer (*12*, *13*).

We report the detection and analysis of the rovibrational spectrum of $[Ar–N_2]^+$ in its $^2\Sigma$ ground state. More than 70 adjacent vibration-rotation lines have been observed around 2272 cm^{-1}, with an intensity distribution that corresponds to a rotational temperature of about 15 K (*13*). The spectrum is that of a $^2\Sigma–^2\Sigma$ transition of a linear molecule and consists of a progression of P- and R-branch doublets, apart from very low rotational quantum numbers where the Q-branch transitions are still intense enough to be detectable. Parts of the spectrum are shown in Fig. 1.

The assignment of these transitions to the molecular nitrogen (NN) stretching vibration of linear $[Ar–N_2]^+$ is straightforward, even though the experiment was not mass selective and other species were produced in the plasma as well. The signal was not observed without Ar or N_2 in the expansion, which excluded pure Ar or N_2 clusters, and scaled linearly with the $[Ar–N_2]^+$ mass signal. The latter signal was strong, as may be expected; the ionization potentials (IPs) of Ar (15.760 eV) and N_2 (15.581 eV) are almost identical (*15*), tending to form a bond with a covalent character upon complexation. Kinetic energy release studies have found a binding energy for $[Ar–N_2]^+$ as high as 1.19 eV, which is comparable, for example, to the value found for the homonuclear species Ar_2^+ (1.29 eV)

Table 1. Molecular parameters describing the rotational (B_v), distortion (D_v), and spin-rotation (γ_v) constants of $[Ar–N_2]^+$ in its electronic $^2\Sigma$ ground state for $v = 0$ and upon vibrational excitation of the NN fundamental ($v = 1$). All values are given in wave numbers. The numbers in parentheses indicate 1σ deviations.

	ν_{01}	B_v	D_v ($\times 10^{-8}$)	γ_v
$v = 0$	0	0.128712(10)	8.9(26)	−0.01065(16)
$v = 1$	2272.2564(2)	0.128212(10)	9.4(22)	−0.01056(16)

Department of Chemistry, Klingelbergstrasse 80, CH-4056 Basel, Switzerland.

*To whom correspondence should be addressed. E-mail: Henricus.Linnartz@unibas.ch